

XMM-Newton Calibration Technical Note

XMM-SOC-CAL-TN-0184

Testing *epspatialcti* on clusters of galaxies

Fabio Gastaldello (*INAF-IASF Milano, Italy*),
Konrad Dennerl (*MPE, Germany*)

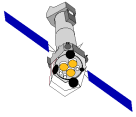
January 3, 2013

1 Scope

This report aims at testing the performance of the SAS task *epspatialcti*. *epspatialcti* corrects an EPIC-pn event file for spatially dependent CTI effects, which remain after the standard CTI correction in SAS has been applied. They show up as pixel to pixel variations in the energy scale. These spatially dependent CTI effects are investigated by measuring spectra of bright extended sources. The task and the associated CCF file have been validated using the Al-K (1.5 keV) and Mn-K (5.9 keV) lines from the internal ^{55}Fe calibration source and the O VII K line (0.6 keV) of the Vela supernova remnant [1]. Here we report the results of the performance of the task when applied to the spectra of bright galaxy clusters.

2 Methodology

We tested the performance of the task *epspatialcti* on the Fe He-like (Fe XXV) $K\alpha$ line at the rest frame energy of 6698.6 eV, the strongest line emission in the spectra of bright, massive galaxy clusters. We followed a similar approach to [1] and extracted images in detector coordinates for singles events with an adaptive binning requiring a fixed number of counts in the 6-8 keV energy band. The boundaries of the regions along the y-axis are aligned with the y ranges covered by the



	6.7 keV
EFF singles	14.1 \rightarrow 12.0
FF singles	11.9 \rightarrow 9.7

Table 1: Standard deviations $\sigma_{\text{before}} \rightarrow \sigma_{\text{after}}$ (in eV) determined in the individual spatial bins after quadratically subtracting the statistical error, before and after running *epspatialcti*.

response matrices. The spectral model consists of a power-law to model continuum and background emission plus a Gaussian line to model the Fe He-like line. In the case of the Perseus cluster an additional line was used to model the Fe H-like (Fe XXVI) line at 6973.1 eV rest frame. Both line energies and width of the Fe XXV line were free parameters. We used the c-statistic on the original 5 eV data bins.

3 Results

3.1 The Perseus cluster

We analyzed the long (125 ks on time) Perseus cluster (at a redshift of $z=0.0179$, so the expected Fe-He line energy is 6586.6 eV) observation (OBSID 0305780101, Extended Full Frame) filtering the observation with a threshold of 0.6 cts s^{-1} for a light curve in 100 s bins in the 10-12 keV energy band (as in [2]). We required 4000 cts in the 6-8 keV range obtaining 65 regions; the fits were performed in the 6-7.3 keV range. Fits were good, with a distribution of $cstat/dof$ with a mean of 1.03 and standard deviation of 0.11 for the spectra before applying *epspatialcti* and a distribution with a mean of 1.02 and standard deviation of 0.09 for the spectra after applying *epspatialcti*; examples are shown in Fig.1.

In Fig.2 we show the results for the spatial distribution of the energies before running *epspatialcti* on the left and on the right after running *epspatialcti*. Following [1], to quantify the amount of suppression obtained with *epspatialcti* we computed the standard deviation of the energies derived for the individual areas after quadratically subtracting the statistical error and the results are summarized in Table 1. The result of $\sigma_{\text{before}} = 14.1 \text{ eV} \rightarrow \sigma_{\text{after}} = 12 \text{ eV}$ can be compared with the result $\sigma_{\text{before}} = 14.2 \text{ eV} \rightarrow \sigma_{\text{after}} = 13 \text{ eV}$ for EFF singles obtained by [1] using the Mn-K line at 5.9 keV from the internal calibration source.

Motivated by the results of the Centaurus cluster (see §3.2) we analyzed an earlier short (51 ks on time) observation of the Perseus cluster taken in Full Frame mode (OBSID 0085110101). The whole observation is affected by soft proton contamination, therefore no flare filtering has been applied (as detailed in [3]). We required 3000 cts in the 6-8 keV range obtaining 28 regions. Performing fits

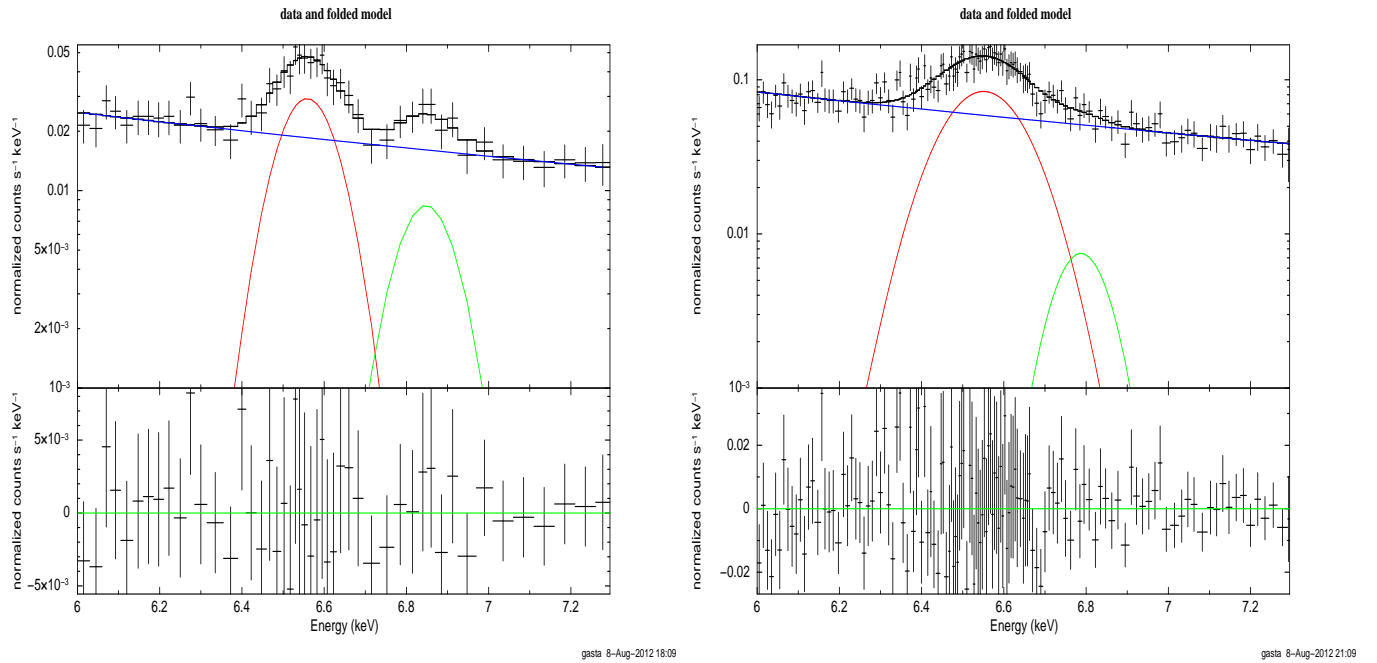
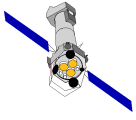


Figure 1: Examples of fit to spectra of the Perseus cluster (single events). *Left panel:* fit to the first bin corresponding to RAW-Y 120-139 of the lower part of the detector. *Right panel:* fit to the sixth bin corresponding to RAW-Y 180-199 of the upper part of the detector.

in the same manner as described above we obtained acceptable fits with a distribution of $cstat/dof$ with a mean of 1.10 and standard deviation of 0.11 for the spectra before applying *epspatialcti* and a distribution with a mean of 1.08 and standard deviation of 0.08 for the spectra after applying *epspatialcti*. We quantified the amount of suppression as done previously, with results summarized in Table 1 and shown in Fig.3.

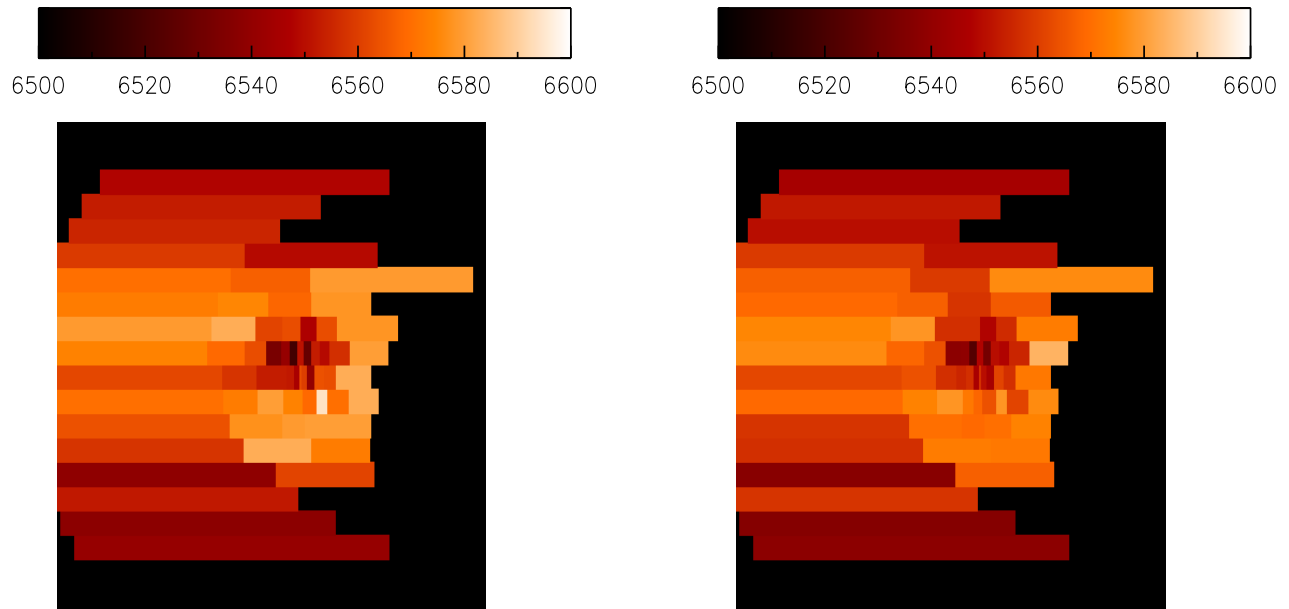
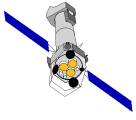


Figure 2: Comparison of the spatially resolved energy determination of the Fe XXV line in the Perseus cluster (expected energy 6586.6 eV at the redshift of the source) for singles in extended full frame mode, before (left) and after (right) running *epspatialcti*. The statistical 1σ error is 5 eV (mean of the distribution of errors for each area, with a standard deviation of 1.7 eV) in both cases. The individual energy determinations exhibit a mean of 6563 eV with a standard deviation of 15 eV before running *epspatialcti* and a mean of 6560 eV with a standard deviation of 13 eV. Taking the statistical uncertainties into account, this corresponds to a standard deviation of 14.1 eV before and 12 eV afterwards.

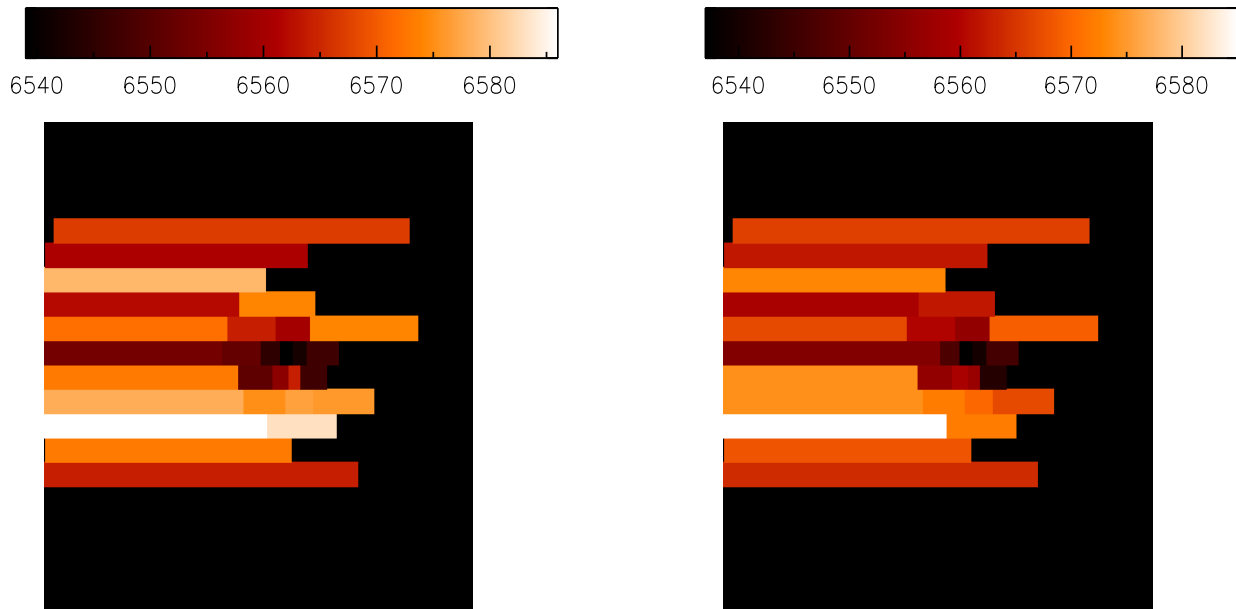
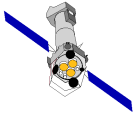
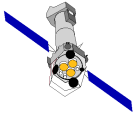


Figure 3: Comparison of the spatially resolved energy determination of the Fe XXV line in the Perseus cluster (expected energy 6586.6 eV at the redshift of the source) for singles in full frame mode, before (left) and after (right) running *epspatialcti*. The statistical 1σ error is 5.3 eV with a standard deviation of 1.9 eV and 5.1 eV with a standard deviation of 1.7 respectively. The individual energy determinations exhibit a mean of 6564 eV with a standard deviation of 13 eV before running *epspatialcti* and a mean of 6561 eV with a standard deviation of 11 eV. Taking the statistical uncertainties into account, this corresponds to a standard deviation of 11.9 eV before and 9.7 eV afterwards.



3.2 The Centaurus cluster

We analyzed two observations of the Centaurus cluster (at a redshift of $z=0.0114$, so the expected Fe-He line energy is 6623.1 eV): one (OBSID 0046340101) taken in Full Frame mode for a good exposure after flare cleaning of 34 ks and the other (OBSID 0406200101) taken in Extended Full Frame mode for a good exposure time of 92 ks. The purpose was to explore on the same astrophysical source the two pn modes; the comparison is somewhat limited by the different statistical quality of the two observations. Given the lower temperature (~ 3 keV) of this cluster compared to Perseus we required only 1000 cts in the 6-8 keV range for the spectral extraction, in order to have a decent number of bins in the short exposure. With these requirements we obtained 17 regions for the short FF observations and 43 for the long EFF observation (this number has been reduced from an initial larger number of ~ 60 regions, some of them a posteriori refused because of very low signal).

For the long EFF observation fits were acceptable with a distribution of $cstat/dof$ with a mean of 1.11 and a standard deviation of 0.09 for the spectra before applying *epspatialcti* and a distribution with a mean of 1.12 and a standard deviation of 0.10 for the spectra after applying *epspatialcti*; examples are shown in Fig.4.

In Fig.5 we show the results for the spatial distribution of the energies before running *epspatialcti* on the left and on the right after running *epspatialcti*. Computing the standard deviation of the energies derived for the individual areas after quadratically subtracting the statistical error is probably not meaningful given the same formal level of standard deviation of the distributions and the statistical errors (as detailed in the caption of Fig.5); given the asymmetry of the error distribution (because of the higher signal of the central regions) if we restrict the analysis to the 23 regions where the statistical error is lower than the median of the distribution of the statistical error we obtain a distribution of individual energy determinations with a mean of 6614 eV and standard deviation of 10.7 eV before applying *epspatialcti* and a distribution with mean 6613 eV and standard deviation 9.5 eV after applying *epspatialcti*. The 1σ error statistical distribution has a mean of 6.5 eV with standard deviation 1.9 eV before *epspatialcti* and a mean of 6.7 eV with standard deviation 2.1 eV after *epspatialcti*. This corresponds to $\sigma_{\text{before}} = 8.6 \text{ eV} \rightarrow \sigma_{\text{after}} = 6.7 \text{ eV}$.

For the short FF observation fits were acceptable with a mean of 1.14 and standard deviation of 0.12 for the fits before *epspatialcti* and a mean of 1.17 and standard deviation of 0.12 for the fits after *epspatialcti*. In Fig.6 we show the plot for the results of the spatial distribution of the energies. The standard deviation of the energies derived for the individual areas after quadratically subtracting the statistical error are summarized in Table 2.

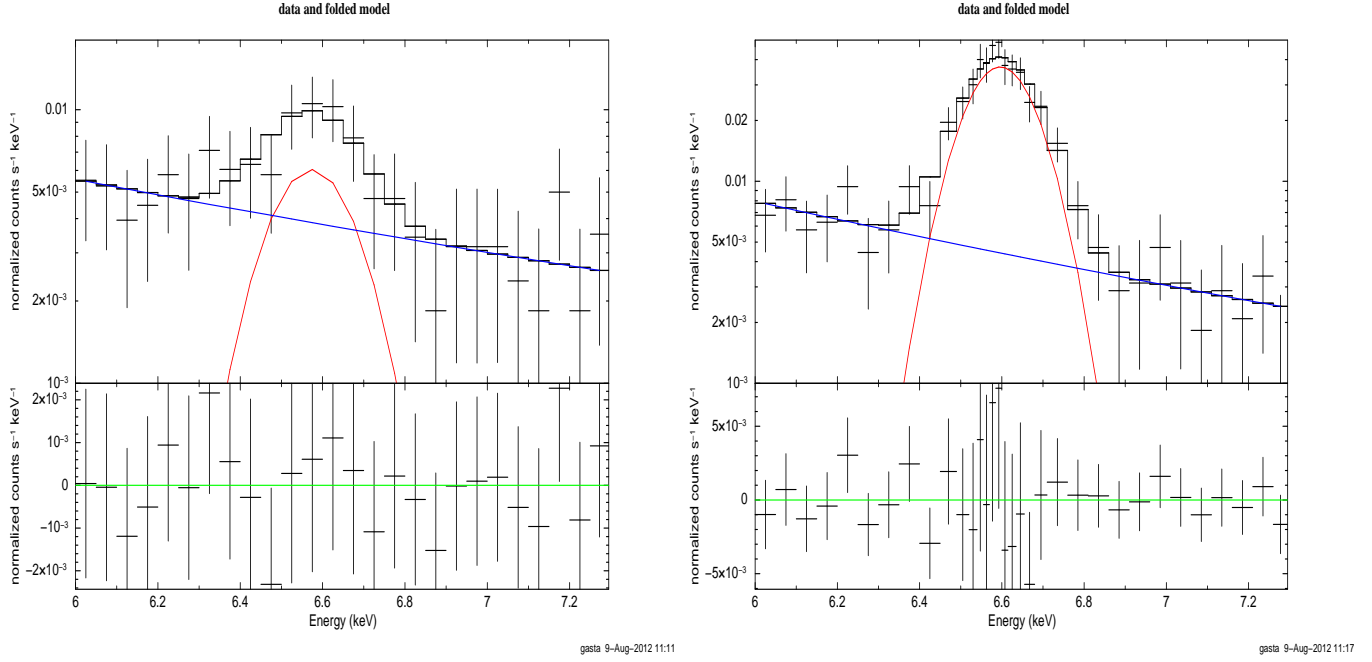
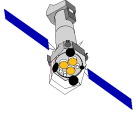


Figure 4: Examples of fit to spectra of the Centaurus cluster (single events) for the long EFF observation (OBSID 0406200101). *Left panel:* fit to the second bin corresponding to RAW-Y 80-99 of the lower part of the detector. *Right panel:* fit to the fourth bin of the column corresponding to RAW-Y 180-199 of the upper part of the detector.

	6.7 keV
EFF singles	7.4 → 7.0
EFF singles restricted	8.6 → 6.7
FF singles	9.0 → 3.1

Table 2: Standard deviations $\sigma_{\text{before}} \rightarrow \sigma_{\text{after}}$ (in eV) determined in the individual spatial bins after quadratically subtracting the statistical error, before and after running *epsptialcti*.

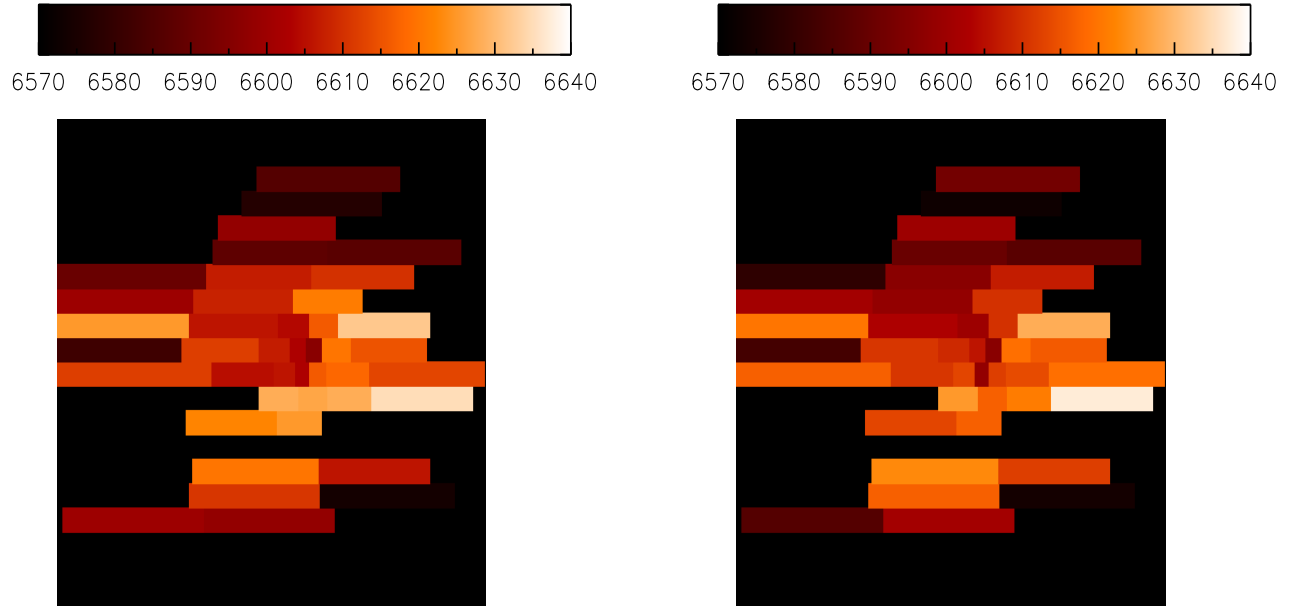
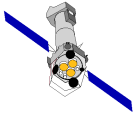


Figure 5: Comparison of the spatially resolved energy determination of the Fe XXV line in the Centaurus cluster (expected energy 6623.1 at the redshift of the source) for singles in extended full frame mode, before (left) and after (right) running *epspatialcti*. The statistical 1σ error is 12.8 eV (mean of the distribution of errors for each area, with a standard deviation of 9 eV; however the distribution is skewed, the median is in fact 9.5 eV and 10 eV for before and after running *epspatialcti* respectively) in both cases. The individual energy determinations exhibit a mean of 6608 eV with a standard deviation of 14.8 eV before running *epspatialcti* and a mean of 6606 eV with a standard deviation of 14.6 eV after running *epspatialcti*. Taking the statistical uncertainties into account, this corresponds to a standard deviation of 7.4 eV before and 7.0 eV afterwards.

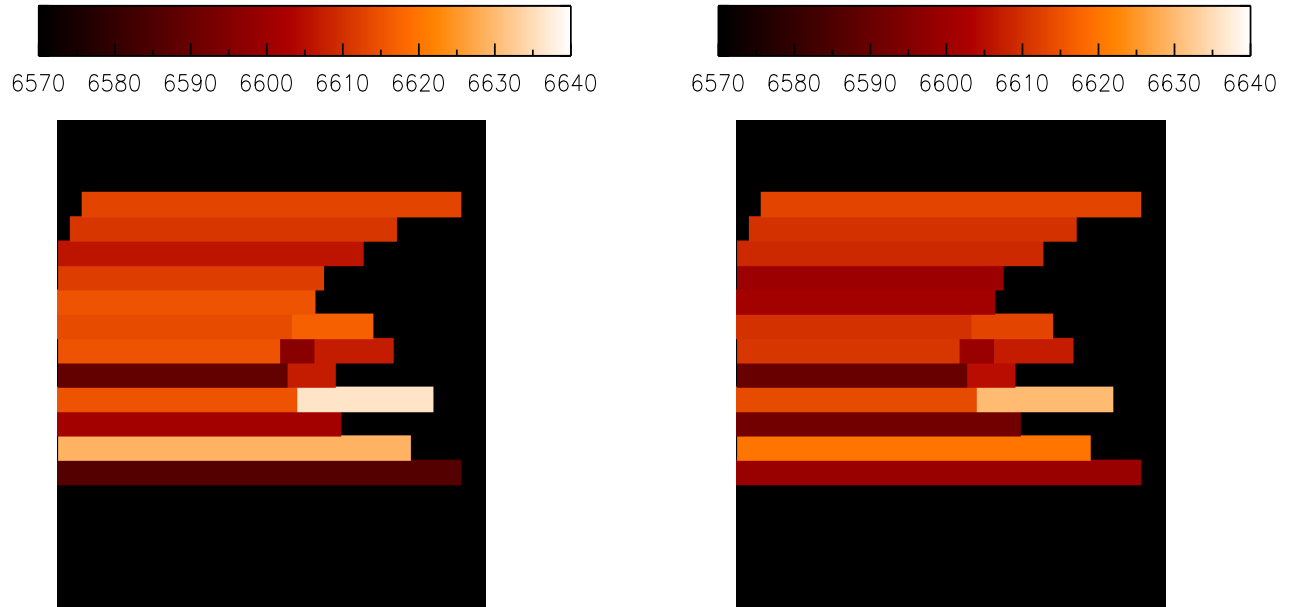
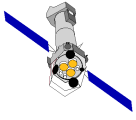
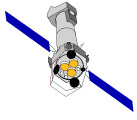


Figure 6: Comparison of the spatially resolved energy determination of the Fe XXV line in the Centaurus cluster (expected energy 6623.1 at the redshift of the source) for singles in full frame mode, before (left) and after (right) running *epspatialcti*. The statistical 1σ error distribution has a mean of 8.7 and standard deviation 3.8 eV for the fits before *epspatialcti* and a mean of 9.4 and standard deviation 4.3 eV for the fits after *epspatialcti*. The individual energy determinations exhibit a mean of 6610 eV with a standard deviation of 12.5 eV before running *epspatialcti* and a mean of 6607 eV with a standard deviation of 9.9 eV after running *epspatialcti*. Taking the statistical uncertainties into account, this correspond to a standard deviation of 9.0 eV before and 3.1 eV afterwards.



4 Conclusions

We provide in this document a test of the performance of the SAS task *epspatialcti* when applied to the spectra of the thermal extended emission of clusters of galaxies. The improvement on the spatial homogeneity of the reconstructed energy of the astrophysical Fe line emission at 6.7 keV is comparable to the one observed in the Mn-K fluorescence line of the internal calibration source.

References

- [1] Dennerl, K. & Saxton, R., 2012, XMM-CCF-REL-283
- [2] Molendi, S. & Gastaldello, F., 2009, A&A, 493, 13
- [3] Gastaldello, F. & Molendi, S., 2004, ApJ, 600, 670